International Journal of Agriculture Innovations and Research 4-2 (2015) 381-389

Evaporation Experimental Study of Liquid Effluent after Methanation

H. Zouaghi
National Engineering School of Monastir
Avenue Ibn El Jazzar, 5019 Monastir – Tunisia
Email: hibazouaghi@yahoo.fr

S. Harmand
University of Lille Nord,
UVHC – LAMIH UMR CNRS 8201
Mont Houy, Valenciennes, Cedex 09, 59300 – France
Email: souad.harmand@univ-valenciennes.fr

S. Ben Jabrallah
Sciences Faculty of Bizerte – Laboratory LETTM
Zarzouna, 7021 Bizerte – Tunisia
sadokjabrallah@yahoo.fr

Abstract – **Pig manure rich in nitrogen, potassium and phosphorus was subjected to anaerobic digestion and phase separation via centrifugation. Several recovery scenarios for the liquid phase of a waste with 2.3% DM (Dry Matter) are analyzed in this paper. The physico-chemical characterization of the effluent is used to justify the use of solar energy in the drying process. The results of an experimental study of the drying kinetics of the effluent using infrared radiation-based drying indicate that evaporated mass flow increases with the increase of heat flux. Several evaporation tests were performed in the laboratory using a solar simulator. The device consists of a stainless steel plate with a tilt angle of 30° that is covered with transparent glass. The liquid circulates as a film on the steel plate and is exposed to a 6000Watt solar simulator. The measured inlet mass flow varied from 0.53 to 1.29g/s.m². The local heat flux measurements, the temperatures and the effluent and water evaporated flow rates are recorded and compared. The measurements indicate that a greater inlet flow results in a lower evaporated flow. The results also demonstrate that preheating the liquid significantly improves the evaporated flow. Comparing drying with and without the cover glass indicates that glass cover ameliorates evaporation and reduces convection heat losses.**

Keywords – **Evaporation, Recovery, Effluent, Flow, Fertilizer.**

I. INTRODUCTION

Due to climate change and the depletion of fossil energy resources, agricultural biogas is of increasing interest. Agricultural biogas has the well-known advantages of reducing greenhouse gas emissions and being a source of renewable energy. In particular, the use of excess animal manure resorption has potential to be a renewable thermal energy source.

In France, the pig industry is concentrated in the area west of Brittany and Pays de la Loire and corresponds to 66% of the national production. Pig manure is a varied source of nutrients and the composition of major elements, such as nitrogen, phosphorus and potassium, as has been well established by many previous studies [2], [3] and [4].

After anaerobic digestion, several studies have been performed to determine the characteristics of the digestate. The question is whether digestate fertilizer is still of value. These analyses indicate that the rate of dry matter increases after anaerobic digestion from 8.1 to 8.9%. Therefore, the rate of organic matter decreases from 59.3 to 44kg/t. The ratio carbon to nitrogen (C/N) is an indicator of the evolution degree of organic matter, which is the material's ability to eventually break down and explains the increase in the C/N ration after methanation. The slurry has a C/N ratio of 4.8. After anaerobic digestion, this ratio increases to 6.2 [5].

Coudure *et al.* conducted a study that investigated the unmixed manure before and after anaerobic digestion. This study considered the average characteristics of the biogas slurry before and after methanation and the efficiency of electricity production via biogas. The pH of the slurry after anaerobic digestion is on average 7.62, which is slightly greater than the pH measured before anaerobic digestion. The average Kjeldahl nitrogen content is 2.38%. The average ammonia nitrogen content is 1.94%. The average of the total nitrogen is 79.8% [6].

The large number of Britannic farms led to the necessity for treatment standards (more than 400 installations in 2008) to reduce the nutrient surpluses from manure. Over three quarters of these installations in France perform biological treatment with phase separation [1]. The thermal energy produced by the biogas plant allows for dehydration of the digestate directly or as a solid fraction after a first mechanical separation phase. This second option is much less energy intensive than the first one. However, this method is best for small surpluses because it allows for removing only a small amount of nitrogen. Indeed, the techniques of centrifugal filtration and decantation are ineffective at removing the soluble components. In addition, methanation promotes the mineralization of nitrogen (and other elements), which is already largely soluble in liquid animal waste [5]. After phase separation, several studies have been performed on possible development scenarios for this effluent after centrifugation. Solar evaporation uses renewable energy and retains most of the nutrients. Based on further analysis of this effluent and references from literature, a value characterizing the liquid was determined.

The most common use of solar energy is solar distillation, given the increasing demand for fresh water in agriculture and industry. Chaker *et al.* [9] studied a spherical distiller for the management of water in arid and remote areas including southern Algeria. They also indicated that solar distillation depends on many factors, including global irradiation, ambient temperature, wind speed and temperature of the water. Their results demonstrated the importance of a transparent Plexiglas cover in the distillation process; the cover reduces losses by convection and promotes evaporation.

Many studies have been performed on water film evaporation in recent years [10], [11] and [12]. Li *et al.* [11] conducted an experimental study of falling water film

evaporation on newly designed enhanced tube bundles and exploited the influence of the Reynolds number on the heat transfer coefficient and temperature on convective heat flux. Schwartze *et al.* [12] studied water film evaporation in moist air with different humidities.

Srithar *et al.* studied the recovery of tannery effluent using an open solar flat collector. This effluent is rich in total dissolved solid, especially chlorides. The aim of their study was to reduce pollution of the land in semi-urban and urban areas. An experimental study to augment evaporation of effluent tannery was conducted. The principle of the study was to increase effluent temperature by passing the effluent over flat plate collector as thin film and then sprinkling it through nozzles to increase the contact area of liquid with air [13], [14] and [15].

Many studies have been performed regarding the heat drying of sludges [16], [17], [18] and [19]. This wastewater has less than 5% DM. The DM contains nutriments and must be recovered. The sludge is collected in a domestic wastewater treatment plant after secondary settling, thickening and belt filter dewatering. Drying experiments were performed by Leonard *et al.* on wastewater having a DM of 20% in a micro-dryer specially designed for handling small individual samples with mass ranging between 0.5 and 5g. The micro-dryer is composed of two parts: the air conditioning and feeding system and the drying chamber. The weighing device is connected to a PC that records the mass every 5s. The micro-dryer can be operated at temperatures ranging between 20 and 180°C. The air superficial velocity in the drying chamber is between 0.3 and 5m/s. They used X-ray microtomography as an innovative technique to follow the evolution of size, shape and texture of soft materials during a drying operation.

The purpose of this study is the recovery of animal effluent rich in nutriment to obtain a product useful in agriculture for soil fertigation.

This work concerns the development of a liquid effluent by thermal evaporation and is divided into two main parts. The first part is a physico-chemical characterization of the effluent. The second part is a study of the drying kinetics of the effluent using an infrared radiation dryer. An experimental study is conducted using a solar simulator. A comparison between evaporated mass flows is made.

II. NOMENCLATURE

C/N	*[-]*	*Ratio Carbon / Nitrogen*
DM	*[%]*	*Dry Matter*
e	*[mm]*	*Thickness*
ICP	*[-]*	*Optical Emission Spectrometry*
IR	*[-]*	*Infrared*
$\dot{m}$	*[g/s]*	*Evaporated flow*
T	*[°C]*	*Temperature*
UV	*[-]*	*Ultraviolet*
X	*[m]*	*Horizontal axis*
Y	*[m]*	*Vertical axis*
Subscripts		
ev		*Evaporated*
in		*Entry*
p		*Plate*
f		*Film (liquid)*

III. EFFLUENT CHARACTERIZATION

Physico-chemical analysis was performed to characterize the product to be treated. The liquid phase of pig manure samples was processed via a methanation and phase separation by centrifugation prior to the analysis. The results of the analysis are presented in **Table I**.

To determine the humidity and dry matter of the sample, the sample was placed in an oven at a temperature of 105°C until the weight stabilized. Determining the rate of organic matter requires calcination of the sample in a furnace after the determination of dry matter, and the mineral matter is the difference between the total content and the organic matter content.

The Kjeldahl method allows for the determination of the total nitrogen. This method involves mixing the sample with concentrated sulfuric acid and a catalyst. The sample is then subject to a temperature ramp and mineralization. Finally, the mineralization of the nitrogen content is achieved after distillation and trapping of the nitrogen in boric acid.

The ammonia nitrogen is determined by nitrogen fixation at a cold temperature by stripping the air from the nitrogen contained in the sample into boric acid. The nitrogen content is then determined in this acid. The determination of urea nitrogen follows the same principle: measuring the nitrogen content in an acid cold sample; however, in this case, the urea nitrogen content is released in the sample through the use of the enzyme urease.

Determining the nutrient levels (phosphorus, potassium, calcium and magnesium) was performed by extracting the sample in hot aqua regia (hydrochloric acid and concentrated nitric acid mixture) and then performing an assay and dosage at the ICP (optical emission spectrometry). The assay follows the ICP measurement principle and is based on the nebulization and the ionization of the liquid sample in argon plasma. The atoms in the sample are excited to a higher energy level.

Table I: Physico-chemical analysis of the digestate after centrifugation

Analysis	**Results on raw (g/100-g)**	**Results on dry (g/kg)**
water content at 105°C	97.7	-
dry matter	2.30	-
organic matter	1.08	468.40
organic carbon	0.54	234.20
pH (21°C)	8.9	-
Fertilizing elements		
C/N ratio	1.70	-
total nitrogen	0.32	138.79
ammonia nitrogen	0.22	95.42
ureic nitrogen	< 0.10	< 43.37
organic nitrogen	0.10	43.37
phosphorus (P_2O_5)	0.048	20.82
potassium (K_2O)	0.61	264.56
calcium (CaO)	0.025	10.84
magnesium (MgO)	0.0029	1.26

The return to steady state is accompanied by the emission of a series of electromagnetic waves in the range of the visible and UV spectrum, which is characteristic of each element. The different wavelengths are separated using a spectrometer. The radiation intensity is proportional to concentration of the element. The analysis results indicated that the fertilizer value of the liquid is still high.

IV. Evaporation of the Liquid Film of Effluent at Rest

A. *Experimental devices*

The device used for this experiment consists of a balance and an infrared dryer manufactured by Sartorius. This dryer is controlled by a computer and allows for the measurement of the mass while changing several parameters, such as temperature and time (Fig. 1.a and 1.b). The balance has an accuracy 10-3g. The temperature of the lamp is between 40 and 160°C.

Once the sample is in place, a plot of the sample mass is shown on the computer using software that is designed to measure the mass as a function of time.

The radiative flux that reaches the surface of the sample is measured using a flow meter connected to a data logger that has an uncertainty of ±0.5mV. The variation of the radiation flux as a function of the temperature of the infrared lamps is shown in Fig. 1.c.

The radiation flux increases with an increase of the temperature of the lamp. There is a maximum of 916.9W/m² when the temperature of the lamp is 160°C.

B. *Experimental results*

Several configurations were performed to study the tendency of the liquid to dry when it is at rest.

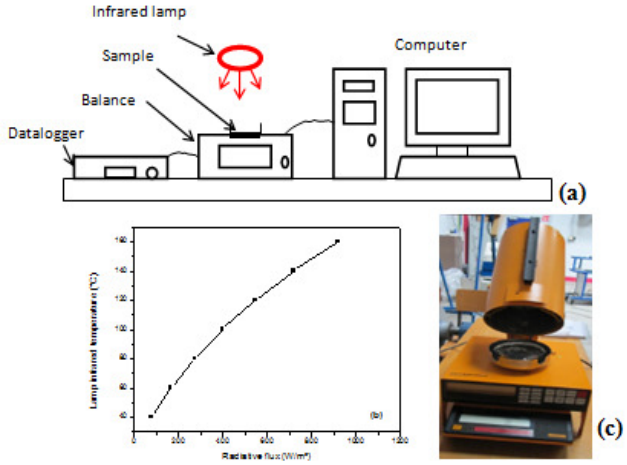

Fig.1. Evaporation test bench for static film effluent: (a) bench test; (b) device photograph; (c) flux curve as function of IR lamp temperature

B.1. Effect of the drying liquid surface to on thickness at a constant temperature

A comparison of the drying rate is performed for two samples having the same thickness but different surfaces while maintaining the heat flux of the infrared radiation source at approximately 916.9W/m².

Table II: Characteristics of the samples

e = 1.1 mm	Volume	Mass	Surface (cm²)
Configuration 1	7.8 ml	7.577 g	78
Configuration 2	4.1 ml	3.325 g	33

We obtained the results shown in Fig. 2.

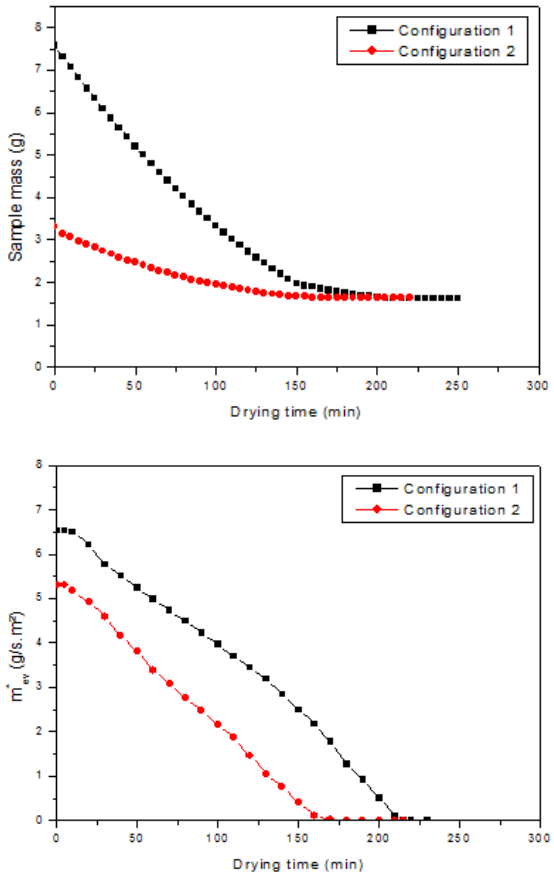

Fig.2. Drying curves for the given configurations

Fig. 2 shows that the drying curve passes through two phases: a phase of rapid decrease of the liquid mass and another with a slow decrease. When the sample is exposed to the infrared radiation, its water content decreases until the mass stabilizes. The evaporated mass flow decreases as a function of time. The maximum of evaporated mass flow is at the beginning of the evaporation process.

A digestate with water content greater than 95% evaporates due to the free water contained in the sample. This process explains the rapid increase in the weight of the digestate. When the water content is between 30-40%, the sample no longer contains free water in its cavities. The remaining material is then considered saturated with bound water, which is difficult to evaporate and requires more energy for evaporation. Therefore, there is a slow decay of the curve until stabilization. This process explains the decrease of evaporated mass flow as a function of time.

The results also indicate that, even if the thickness of the sample remains constant, samples having a greater portion of water will take longer to dry.

The configurations shown in Table III were considered. The samples were dried at a heat flux of 916.9W/m².

Table III: Sample characteristics

Volume = 7.8 ml	**Surface (cm²)**
Configuration 1: e = 1.1mm	71
Configuration 3: e = 2.3mm	33

The results indicate that the drying times of the two samples are very similar. A sample from configuration 3 has a drying time of 255min. This result shows that the thickness of the liquid has no influence on the drying kinetics because the drying remains a surface phenomenon.

In the remainder of the work, configuration 2 is used, and a varying infrared lamp temperature is used.

B.2. Effect of the lamp temperature with a constant temperature and area

In configuration 2, the drying time is the minimum. This configuration is used in the following tests. The sample is dried at different heat fluxes of the IR lamp.

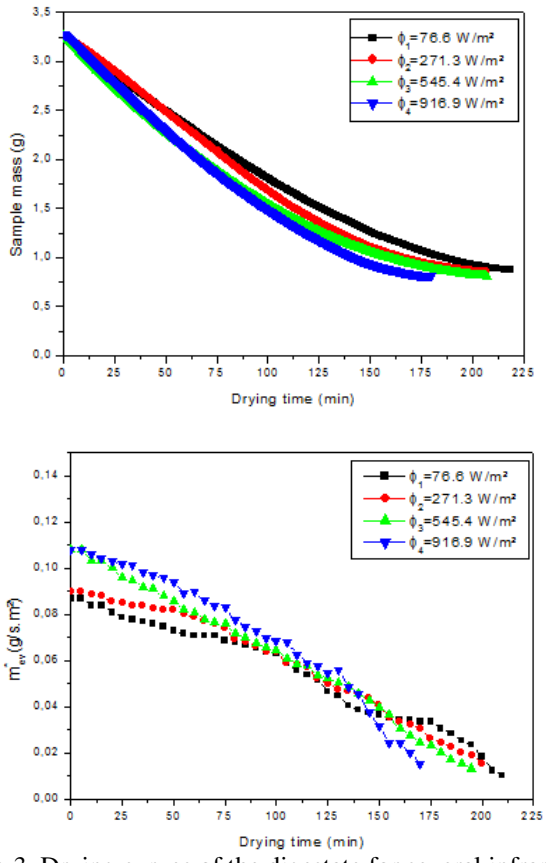

Fig.3. Drying curves of the digestate for several infrared lamp heat fluxes

The drying curves have the same features. The curves have two phases: a fast decay phase and slowly decaying phase. We discover that, when the temperature of the lamp is higher, the drying is faster. The drying time is a minimum when the flux is approximately 916.9W/m². At this temperature, the final weight was 0.867g.

When we introduce the liquid to dry, its temperature increases, thereby increasing the evaporated mass flow. Subsequently, the mass flow decreases. When the heat flow is at its maximum, the maximum evaporated flow occurs in the first part of the decreasing curve. When the drying time is between 130 and 150min, the minimum evaporated mass flow occurs when the heat flux at its maximum. Thus, the evaporated mass flow depends on the heat flux until 130min; subsequently, the evaporated mass flow is inversely proportional to the heat flux.

The evaporated mass flow can be presented according to Fick's law as the opposite of the concentration gradient between the water vapor in the air and that at the interface of liquid film. At t=0s, the air is supposed dry; its vapor concentration is low, so evaporated mass flow is at its maximum. During the evaporation process, vapor released from the liquid makes the air more saturated, which explains the decrease of the evaporated mass flow.

Figure 4 presents increases of the maximum and average of the evaporated mass flow for different heat fluxes. The maximum is 0.11g/s.m² for a heat flux of 917W/m². The average of evaporated mass flow is 0.07g/s.m² for the same heat flux. The evolution of the evaporated mass flow is related to the heat flux. It increases with the increase of the heat flux.

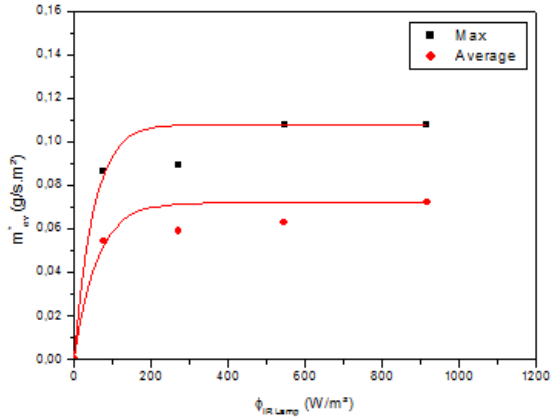

Fig.4. Average and maximum evaporated mass flow for different IR lamp heat fluxes

V. Evaporation of Flowing Liquid Film of the Effluent

A. Experimental device

This process consists of flowing the aqueous liquid effluent on an inclined plate subject to solar flux. The purpose is to produce solid fertilizer from aqueous liquid waste, such as anaerobic digestate. The system should be inexpensive and consume as little energy as possible to enable widespread adoption of the system by farmers who make methane.

This device is an evaporator composed of stainless steel plate with a tilt angle of 30°. This plate is 2m long and 1m wide. The plate is covered by a pane of heat-resistant glass having a thickness of 6mm. The liquid is injected from the top of the plate with an injection nozzle. Fluid flows along the plate and is recovered in a gutter (Fig. 5.a).

The steel plate is insulated on the underside with glass wool. The steel plate is heated using a 6000W solar simulator. The solar simulator is placed parallel to the plate at a distance of 2m, such that heat flux is focused on of the upper part of plate at a flux density similar to that of the sun.

Thermocouples were fixed to the stainless steel plate, as shown in Fig. 5.b. The thermocouples are positioned into three rows of nine lines. The first line of thermocouples is approximately 20cm from the top and 15cm for the edge. The thermocouples are spaced at a distant of 20cm. K-type thermocouples used in this study had a margin of error of ± 2.5°C.

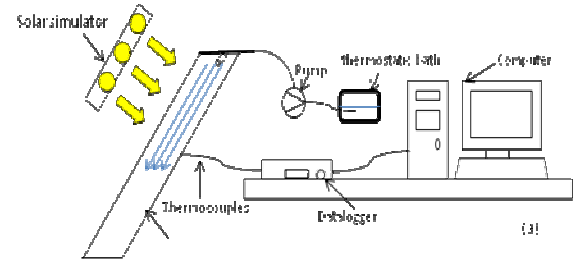

(a)

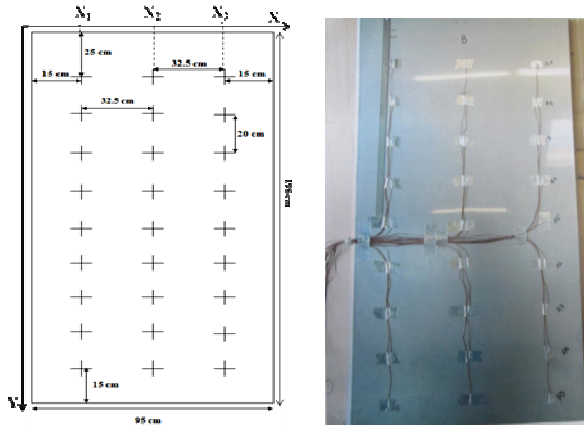

(b)

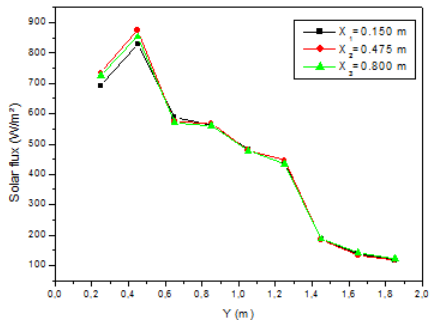

(c)

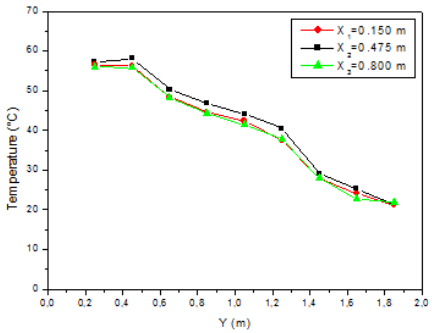

(d)

Fig.5. (a) Schematic diagram of the evaporator; (b) layout of thermocouples on the plate; (c) cartography of flux; (d) plate temperature profile

Once steady state is achieved, the liquid was injected from the top of the plate using a pump that feeds dispense manifold. The inlet mass flow measurement was performed by weighing the liquid before and after injection for a predetermined time before the start of solar simulator.

The evaporated mass flow was measured when the solar simulator was powered and after stabilization of the temperature. The measurement was performed by weighing the liquid at the outlet of plate over a given time. The uncertainty of the mass flow measurement is approximately 13%, as determined by the uncertainties of the balance and the time period measurement.

In another set of measurements, the same tests will be performed by removing the glass cover. Thus, the plate is directly exposed to solar simulator. The results of these measurements and the tests with the cover are compared.

The cartography of the flux is shown in **Fig. 5.c**. We chose the same points as the thermocouples (three columns of nine lines). The solar flux is measured using a pyranometer with accuracy ±4–10µV/W/m².

The maximum flux is at Y=0.45m, according to the different positions X_1, X_2 and X_3. The flux is 874W/m² at Y=0.45m for position X_2. The minimum flux is 116W/m² at Y=1.85m for position X_1. The mean flux along the plate is approximately 452W/m².

The temperature profile of the steel plate when steady state is reached is shown in **Fig.5.d**. Because the heat flux of solar simulator is focused on the second column, the temperatures are the greatest at that column. When x=45cm, the plate temperature is greater.

At steady state, the maximum temperature of the glass is approximately 40°C.

B. Experimental results

The total heat flux presents the sum of the solar simulator heat flux, with an average of approximately 452W/m², and the heat flux from the preheated liquid. The heat flux required for liquid preheat is calculated using Q=mCpΔT. The calorific capacity of the digestate is constant over temperature ranges of 20 to 67.5°C and has an average of 0.166J/g.°C, which is much less than that of water, which has an average of approximately 4.08J/g.°C for the same temperature range.

A solar drier was used by Hongfei *et al.* [7] for the desalination of water. This plate was inclined by 20°. The plate area was approximately 1m². The plate was covered with double glazing. Hongfei et al. used a 1000W solar simulator. They found that evaporated mass flow increases with the increase of heat flux. Tests were performed with three different heat fluxes and varying the inlet mass flow. The best evaporated flow is approximately 0.24g/s for 665W/m² and a minimum inlet flow of 0.85g/s. As a result, if the inlet mass flow is low and the heat flux is high, then the evaporated mass flow is higher.

To compare the results with those of Hongfei *et al.*, tests are conducted by evaporating a water film flowing on the plate covered with glass for various illumination powers and various inlet temperatures of the liquid.

The total heat flux represents the sum of the simulator heat flux and the heat flux required to preheat the liquid to allow it to evaporate. The results are presented in **Fig. 6**.

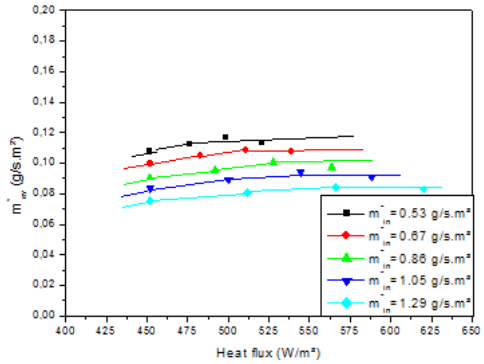

Fig.6. Representative curves of the evaporated water flow as a function of the heat flux

The maximum evaporated mass flow of water is approximately 0.115g/s.m² when the inlet mass flow is 0.53g/s.m² for total heat flux of 476W/m². Evaporated mass flow increases when heat flux is between 452 and 500W/m². The best evaporated mass flow is 0.12g/s.m² for an input of 0.53g/s.m². At 521W/m², the evaporated mass flow remains constant. The fluid behaves as if it was heated to between 452 and 500W/m². The same tests were performed for liquid effluent. The results are presented in Fig.7.

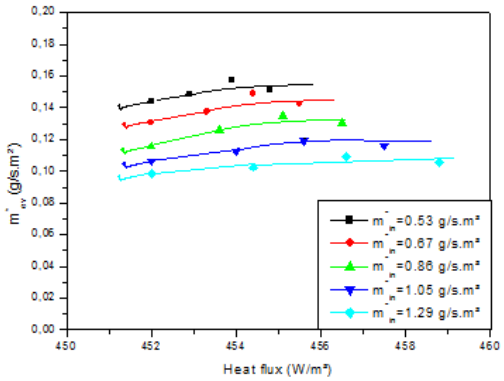

Fig.7. Variation of the evaporated mass flow of the effluent as function of the heat flux for different inlet mass flows

The evaporated mass flow of the effluent increases when the total heat flux increases and when the inlet mass flow decreases. The evaporated mass flow is at its maximum when total heat flux is 455W/m².

The maximum evaporated mass flow is 0.155g/s.m² when the inlet mass flow is 0.53g/s.m² if the liquid is heated to 454W/m². Whereas, at 454W/m², the evaporated mass flow is 0.158g/s.m² for the same inlet flow.

The results indicate that, for the same inlet temperature, at various heat fluxes for water and the effluent, the latter has a better evaporation rate. Because the calorific capacity of the effluent is lower, it requires less heat flux to be heated to the same temperature compared to water.

Next, the plate was directly exposed to solar simulator, and then we repeated the same tests. A comparison of these results to the previous results is presented in Fig.9.

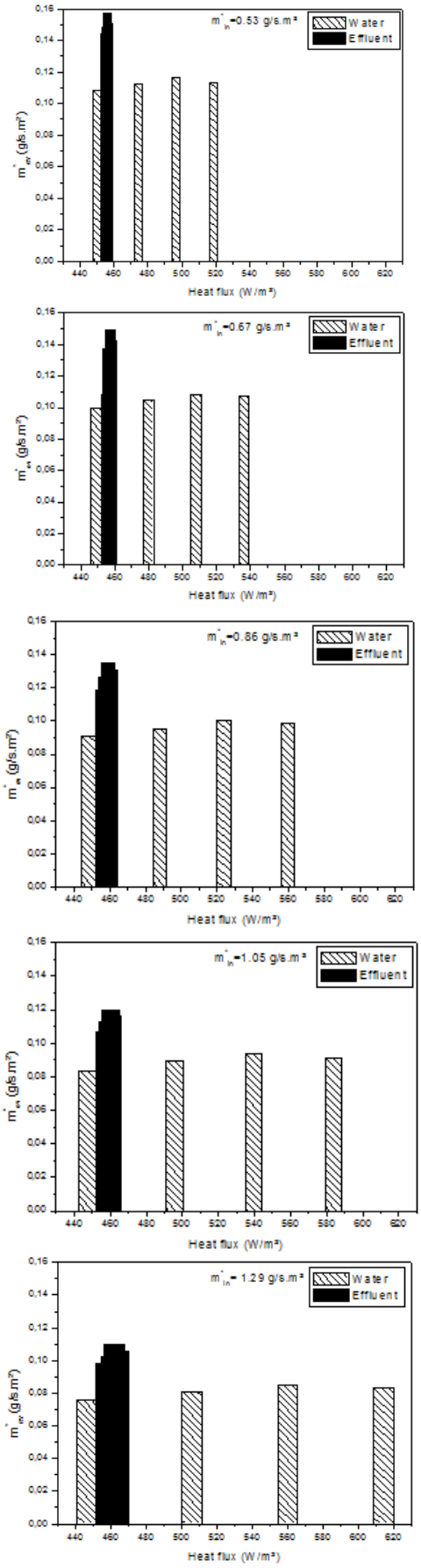

Fig.8. Comparison between the evaporated mass flows of water and effluent

The evaporated flow reaches its maximum when the inlet flow is at its minimum. In addition, the tests with a glass cover were found to have improved performance because the glass cover ameliorated the evaporated flow. Therefore, evaporation is not only related to heat flux but also to the glass cover. Note that the best evaporated flow is when the effluent is heated at 454W/m² and when a cover glass is used. For a minimal inlet flow of 0.53g/s.m², the evaporated flow is approximately 0.155g/s.m², compared to the flow of 0.105g/s.m² obtained when the plate is not covered with glass under the same conditions. The evaporated flow decreases with the increase of the inlet flow.

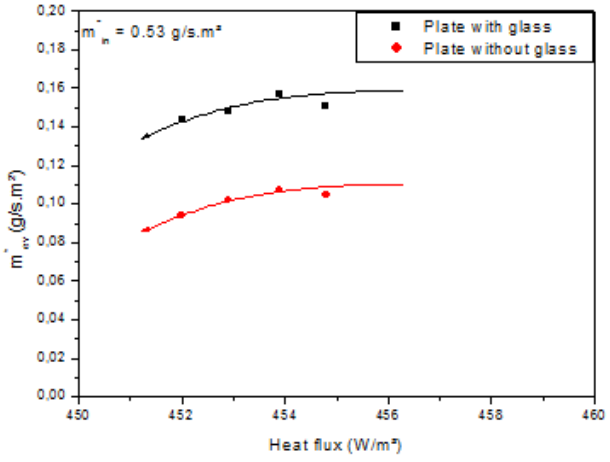

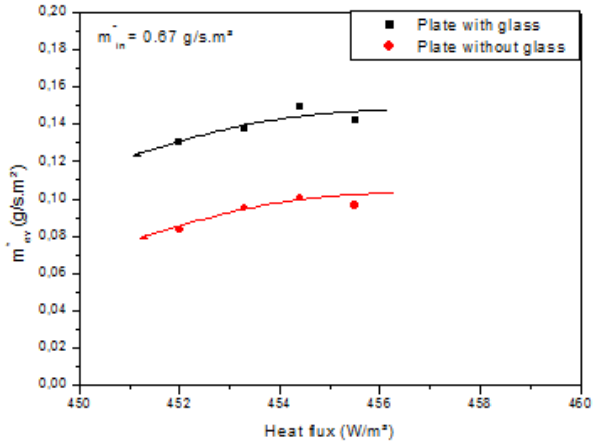

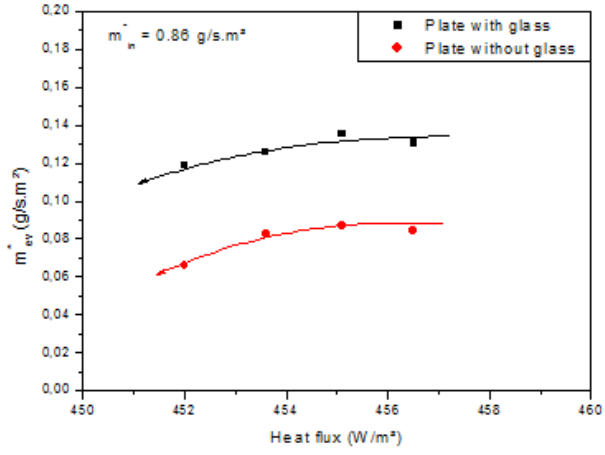

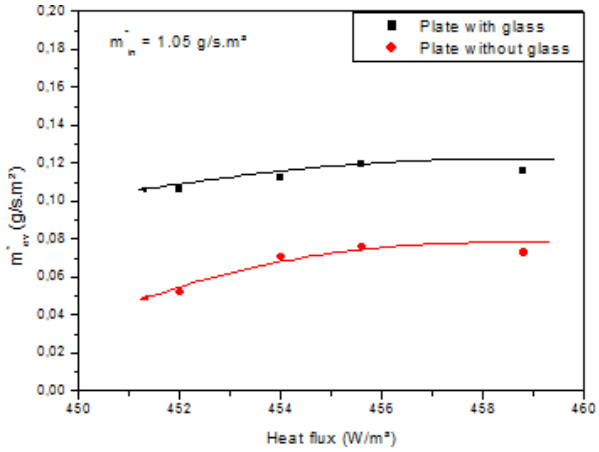

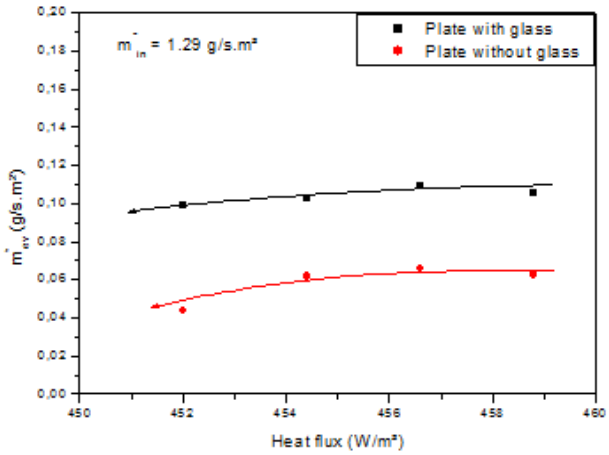

Fig.9. Comparison between the evaporated mass flow of the effluent when the plate is used with and without the glass cover

Dufresne [8] is among the researchers who studied this phenomenon. He explained that the glass allows the solar radiation to pass while absorbing all of the infrared radiation. Thus, the glass absorbs the infrared radiation emitted by plate and is heated. As the glass temperature increases, it emits itself more infrared radiation; as a result, its temperature will increase until it loses as much energy as it receives. The radiation emitted by the glass is half emitted to the outside and lost, with the rest partly absorbed by the plate. Because the plate is now receiving more energy than it loses, its temperature will rise until it loses as much energy as it receives. This infrared radiation emitted by the extra plate is absorbed by the glass. These rays are transmitted several times until equilibrium is reached, wherein the plate temperature is higher than in the device without glass. As a result, the evaporated flow in better when the glass is used. This effect of the glass is the greenhouse effect. The purpose of the glass is to let radiation pass and inhibit the dissipation of the heat that forms between plate and glass under the influence of sunlight. The glass is used to limit the heat loss between the glass and the air and between the liquid and the air.

The evolution of the evaporated mass flow for different drying modes is summarized in Fig. 10.

Using an infrared lamp, the evaporated mass flow increases with the increase of the heat flux. The maximum

evaporated mass flow is approximately 0.1g/s.m² for a heat flux of 400W/m². The average of the evaporated mass flow is 0.06g/s.m² for the same heat flux. Comparing the solar simulator setups, the evaporated mass flow is better when the plate is used with the glass cover. The maximum evaporated mass flow is approximately 0.11g/s.m² when the plate is used without a glass cover and is 0.14g/s.m² when the plate is used with a glass cover.

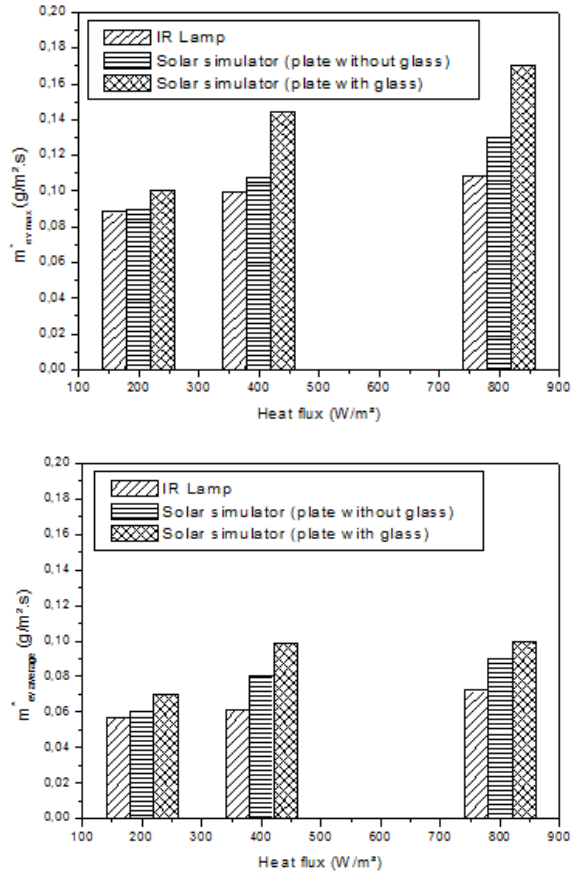

Fig.10. Variation of the average and maximum mass flows for different heat fluxes and for different drying modes

The average of the evaporated mass flow is approximately 0.06 g/s.m² when the plate is used without a glass cover and approximately 0.14g/s.m² when the plate is used with a glass cover for the same heat flux.

VI. Conclusion

A study of the liquid phase behavior of pig manure digestate, which is rich in nutrients, was conducted. The digestate drying kinetics at rest indicated that this phenomenon is not dependent on the thickness of the sample but is a surface phenomenon.

A study was performed on the evaporation of a digestate flowing down a film on a 30° inclined plate for different heat fluxes and the inlet temperatures of the liquid. A preliminary study using tap water was conducted. The same phenomenon was observed when a digestate was used. The evaporated mass flow was found to increase with a decrease in the inlet flow and with an increase in the total heat flux. Comparing the evaporation of the two liquids, water requires more power to be evaporated because of the low heat capacity of the effluent.

The plate temperature is higher when the plate is used with a glass cover, than its temperature when the plate is used without the glass cover. Therefore, the evaporated flux is better when the plate is used with the glass cover because the glass reduces heat losses due to convection. Using a glass cover, the evaporated mass flow is better when the inlet mass flow is the lower than 0.53g/s.m² and the plate is exposed to a total heat flux of 454W/m².

Evaporation using solar simulator increases the dry matter content of liquid from approximately 2.3% to 30%. Using the same heat flux of the IR lamp, the obtained product is free of water. The choice of the method of effluent evaporation depends on the nature of the fertilizer and agricultural soils.

Acknowledgment

This research is a part of a Ph. D study in National Engineering School of Monastir in Tunisia. It's supported by the laboratory TEMPO of the University of Valenciennes and Hainaut Cambresis and the laboratory of Energy, heat and mass transfer (LETTM) of Sciences Faculty of Bizert in Tunisia.

References

[1] Levasseur P, 2010. Déshydratation des digestats de méthanisation Analyse économique de quatre procédés. La revue technique de l'IFIP, TechniPorc, Vol. 33, N°5, 2010.

[2] Granier R, Texier C, 1993. Production du lisier de porc à l'engrais : quantité et qualité. Techni-porc, mars 1993, p 23-31.

[3] Latimier P, Gallard F, Corlouër A, 1996. Actualisation des volumes et des quantités d'azote, de phosphore et de potasse rejetés dans le lisier par un élevage naisseur-engraisseur. Journées Rech. Porcine en France, 28 : 241-248.

[4] Levasseur P, 1998. Composition et volume de lisier produit par le porc : Données bibliographiques. TECHNI - Volume 21, n°4, 1998 : p 16 – 19.

[5] Oost JFr, De Toffoli M, 2009. Estimation de la valeur fertilisante de digestats issus de la biométhanisation. Résultat de 3 années d'expérimentation en culture de maïs (2009 à 2011), 5 p.

[6] Coudure R, Castaing J, 1997. Bilan de fonctionnement d'une unité de méthanisation de lisier de porc. Journées Rech. Porcine en France, 29, p 335-342.

[7] Hongfei Z, Xinshi G, 2002. Steady-state experimental study of a closed recycle solar still with enhanced falling film evaporation and regeneration. Renewable Energy 26 (2002), p 295 – 308.

[8] Dufresne J. L, C. Youinou, 2007. Cent réponses sur le réchauffement de la planète, Tournon, (2007), 120 p.

[9] A. Chaker 1 et G. Menguy, 2001. Efficacité Interne d'un Distillateur Solaire Sphérique. Revue Energies Renouvelables : Journées de Thermique (2001) 53-58.

[10] Jingchun Min, Yicun Tang, 2015. Theoretical analysis of water film evaporation characteristics on an adiabatic solid wall. International journal of refrigeration 53 (2015) 55e61.

[11] Li, W., Wu, X.Y., Luo, Z., Webb, R.L., 2011. Falling water film evaporation on newly-designed enhanced tube bundles. Int. J. Heat. Mass Transf. 54, 2990e2997.

[12] Schwartze, J.P., Brocker, S., 2000. The evaporation of water into air of different humidities and the inversion temperature phenomenon. Int. J. Heat. Mass Transf. 43, 1791e1800.

[13] Srithar, K. Mani, A., 2003. Comparison between simulated and experimental performance of an open solar flat plate collector for treating tannery effluent. International Communication in Heat and Mass Transfer 30 (4), 505-514.

[14] Srithar, K. Mani, A., 2004. Analysis of a single cover FRP flat plate collector for treating tannery effluent. Applied Thermal Engineering 24 (5-6), 873-883.
[15] Srithar, K. Mani, A., 2007. Open fibre reinforced plastic (FRP) flat plate collector (FPC) and spray network systems for augmenting the evaporation rate of tannery effluent (soak liquor). Solar energy 81 (2007) 1492-1500.
[16] A. Leonard , S. Blacher, P. Marchot , M. Crine, 2006. Use of x-ray microtomography to follow the convective heat drying of wastewater sludges. Drying Technology 20 (4&5), 1053–1069.
[17] A. Léonard , S. Blacher, P. Marchot, J. P. Pirard, M. Crine, 2004. Measurement of Shrinkage and Cracks Associated to Convective Drying of Soft Materials by X-ray Microtomography. DRYING TECHNOLOGY Vol. 22, No. 7, pp. 1695–1708, 2004.
[18] A. Leonard, S. Blacher, P. Marchot, J.-P. Pirard, and M. Crine, 2005. Convective Drying of Wastewater Sludges: Influence of Air Temperature, Superficial Velocity, and Humidity on the Kinetics. Drying Technology, 23: 1667–1679, 2005.
[19] J. Vaxelaire, J. M. Bongiovanni, P. Mousques and J. R. Puiggali, 2000. Thermal drying of residual sludge. Wat. Res. Vol. 34, No. 17, pp. 4318±4323, 2000.